

# Exciton induced directed motion of unconstrained atoms in an ultracold gas

K. Leonhardt,<sup>1</sup> S. Wüster,<sup>1,2</sup> and J. M. Rost<sup>1</sup>

<sup>1</sup>Max Planck Institute for the Physics of Complex Systems,  
Nöthnitzer Strasse 38, 01187 Dresden, Germany

<sup>2</sup>Department of Physics, Bilkent University, Ankara 06800, Turkey

We demonstrate, that through localized Rydberg excitation in a three-dimensional cold atom cloud, atomic motion can be rendered directed and nearly confined to a plane without external constraints for the motion of individual atoms. This enables non-adiabatic electronic dynamics of Rydberg atoms accelerated by dipole-dipole interactions under natural conditions, and their observation. Using the full  $l = 0, 1$   $m = 0, \pm 1$  angular momentum state space, our simulations show that conical intersection crossings are clearly evident, both in atomic mean position information and excited state spectra of the Rydberg system. This suggests flexible Rydberg aggregates as a test-bench for quantum chemical effects in experiments on much inflated length scales.

PACS numbers: 32.80.Ee, 82.20.Rp, 34.20.Cf, 31.50.Gh

**Introduction:** Electronic Rydberg excitation in ultra cold gases creates highly controllable quantum systems with promising applications that take advantage of the extreme interactions among Rydberg atoms [1]. Prominent examples include quantum information [2–5], the simulation of spin systems [6–8] and many more processes with controlled electron correlation. Typically, for these applications the atomic gas is assumed to be “frozen”. The unavoidable (thermal) motion of the atoms constitutes then a limiting source of noise and decoherence [9, 10].

Yet we know, that in every molecule bound atomic and electronic motion are entangled in coherent dynamics. Analogously, atoms of an ultra cold gas – energetically in the continuum – can be turned from a noise source into an asset using flexible Rydberg aggregates [11–16]. Rydberg excitation realised as an exciton that entangles two or more atoms exerts a well defined mechanical force on the atoms which start to move. The resulting directed motion of a few Rydberg atoms in a prescribed, dimensionally reduced geometry [15–25] enables transport of electronic coherence along with atomic mechanical momentum involving quintessential quantum chemical processes such as conical intersections (CI) [18, 25, 26]. Thereby, transport of energy and entanglement could be ported from the (chemical)  $nm$  scale to spatial distances of  $\mu m$  [16, 17, 27], allowing for direct and detailed optical monitoring [14, 28–31] of quantum many-body state dynamics. While eventually possible in tight atom traps of experiments in the future, the dimensionally reduced environment has not only been an experimental restriction but also a principal one in our quest to take chemical coherence of atoms bound in molecules to atoms moving in the continuum.

In the following, we will show how to lift this restriction by demonstrating that if *initiated in a low dimensional space* entangled molecular motion in the continuum will remain confined to this space despite the possibility for all particles (ions and electrons) to move in full space. Together with advances in the newest generation exper-

iments on Rydberg gases beyond the frozen gas regime, involving microwave spectroscopy [32] or position sensitive field ionisation [33], our results enable the quantum simulation of chemical processes in flexible Rydberg aggregates as an experimental science. These recent efforts [32, 33] extend earlier pioneering studies of motional dynamics in Rydberg gases [34–42] and now render the rich dynamics of Rydberg aggregates fully observable.

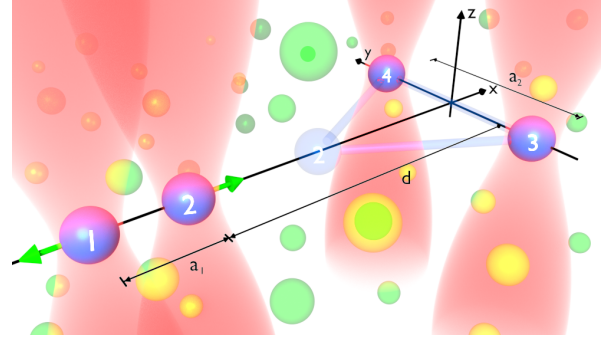


FIG. 1: (color online) Embedded flexible Rydberg aggregate. Four excitation beams (red shades) define focus volumes in which exactly one atom is excited to a Rydberg state (blue balls, 1-4), within a cold gas (green balls). Our co-ordinate system has its origin at the mean position of atom 1, several geometrical parameters are explained in the text. Subsequent to Rydberg excitation, dipole-dipole interactions will cause acceleration along the green arrows, causing atom 2 to reach the position shown in light blue, where a CI will cause strong non-adiabatic effects.

A central element of the Rydberg aggregate, non-adiabatic motional dynamics on several coupled Born-Oppenheimer surfaces [18, 25], is now experimentally accessible, as we show here.

To be specific, we investigate in this letter a flexible Rydberg aggregate consisting of  $N = 4$  Rydberg  $^7\text{Li}$  atoms (mass  $M = 11000$  au), excited to principal quantum number  $\nu = 80$ , embedded within a host cold atom cloud of ground-state atoms, see FIG. 1. This setup is

created with tightly focussed Rydberg excitation lasers. We assume that the focus volumes are small enough to deterministically excite just a single atom within each to an angular momentum  $l = 0$  Rydberg state  $|s\rangle$ , exploiting the dipole-blockade [2, 3].

As shown in FIG. 1, the Rydberg atoms attain a T-shaped configuration after excitation, defined by laser foci centered on the mean position  $\mathbf{R}_0^{(n)}$  for atom  $n$ . We place the origin of our coordinate system at  $\mathbf{R}_0^{(1)}$ , such that other focus positions shown in the figure are  $\mathbf{R}_0^{(2)} = a_1 \mathbf{e}_x$ ,  $\mathbf{R}_0^{(3)} = (a_1 + d)\mathbf{e}_x - a_2 \mathbf{e}_y/2$  and  $\mathbf{R}_0^{(4)} = (a_1 + d)\mathbf{e}_x + a_2 \mathbf{e}_y/2$ , where  $\mathbf{e}_\xi$  with  $\xi \in \{x, y, z\}$  is the unit vector in the  $\xi$ -direction. The geometrical parameters employed here are  $a_1 = 10 \mu\text{m}$ ,  $a_2 = 37 \mu\text{m}$  and  $d = 51 \mu\text{m}$ . Importantly, inter-atomic separations span a two-dimensional (2D) plane in 3D space. We will refer to atom 1 and 2 as the horizontal Rydberg dimer and atoms 3 and 4 as the vertical Rydberg dimer. The positions of all Rydberg atoms are collected into the vector  $\mathbf{R} = (\mathbf{R}^{(1)}, \dots, \mathbf{R}^{(N)})^T$ . Co-ordinates of ground-state atoms are not required since these will be merely spectators for the dynamics of Rydberg atoms, as shown in [21] and found experimentally in [32, 33]. We allow for entirely unconstrained atomic motion in three dimensions, Rydberg atom angular momentum states  $l = 0, 1$ ;  $m = 0, \pm 1$  and the anisotropy of dipole-dipole interactions.

*Anisotropic dipole-dipole interactions:* Following laser excitation, exactly one of the four atoms is transferred to an  $l = 1$  state  $|p, m\rangle$  with a specific azimuthal quantum number  $m$ , using a microwave as discussed further below. This will introduce resonant dipole-dipole interactions into the system.

We work in an electronic Hilbertspace, in which all atoms are in  $|s\rangle$ , except the one in  $|p, m\rangle$ . This allows us to expand the electronic wavefunction in the basis  $\mathcal{B} = \{|\pi_\alpha, m\rangle\}_{m=-1,0,1}^{\alpha=1,\dots,N}$ , where  $|\pi_\alpha, m\rangle = |s \dots (p, m) \dots s\rangle$  denotes the state where the  $\alpha$ th atom is in the state  $|p, m\rangle$ . We thus neglect spin-orbit coupling, which is a good approximation for Lithium [43, 44].

Our effective electronic Hamiltonian model captures the essential features of atomic interactions,  $\hat{H}_{\text{el}}(\mathbf{R}) = \hat{H}_{\text{dd}}(\mathbf{R}) + \hat{H}_{\text{vdW}}(\mathbf{R})$ , with  $\hat{H}_{\text{dd}}(\mathbf{R})$  containing the resonant dipole-dipole interactions between two atoms in different states ( $sp$ ) and  $\hat{H}_{\text{vdW}}(\mathbf{R})$  containing the non-resonant van-der-Waals (vdW)-interactions between two atoms in the same state ( $ss$  or  $pp$ ). The resonant contribution is given by

$$\hat{H}_{\text{dd}}(\mathbf{R}) = \sum_{\substack{\alpha, \beta=1; \\ \alpha \neq \beta}}^N \sum_{m, m'=-1}^1 V_{m, m'}(\mathbf{R}_{\alpha\beta}) |\pi_\alpha, m\rangle \langle \pi_\beta, m'|, \quad (1)$$

where  $\mathbf{R}_{\alpha\beta} = \mathbf{R}^{(\alpha)} - \mathbf{R}^{(\beta)}$  and the dipole-dipole transi-

tion matrix element [45]

$$V_{m, m'}(\mathbf{r}) = -\sqrt{\frac{8\pi}{3}} \frac{\mathfrak{d}^2}{|\mathbf{r}|^3} (-1)^{m'} \times \begin{pmatrix} 1 & 1 & 2 \\ m & -m' & m' - m \end{pmatrix} Y_{2, m'-m}(\vartheta_{\mathbf{q}}(\mathbf{r}_{\mathbf{q}}), \varphi_{\mathbf{q}}(\mathbf{r}_{\mathbf{q}})), \quad (2)$$

where  $Y_{lm}(\vartheta, \varphi)$  are spherical harmonics and their prefactor the Wigner-3j symbol. We denote the radial matrix element with  $\mathfrak{d} = \mathfrak{d}_{\nu, 1; \nu, 0}$  for a transition  $|\nu s\rangle \rightarrow |\nu p\rangle$ ,  $\mathfrak{d} = 8250$  for  $\nu = 80$ . The angles  $(\vartheta_{\mathbf{q}}, \varphi_{\mathbf{q}})$  are the polar and azimuthal angle of the vector  $\mathbf{r}_{\mathbf{q}} = \mathbf{Q} \cdot \mathbf{r}$ , which is the atomic separation  $\mathbf{r}$  expressed in a rotated cartesian co-ordinate system, obtained from the one in FIG. 1 by application of the rotation matrix  $\mathbf{Q}$ . The  $z$ -axis of this system defines the quantisation axis. We will consider two choices for our quantisation axis  $\mathbf{q}_z = \mathbf{Q} \cdot \mathbf{e}_z$ , namely  $\mathbf{q}_z = \mathbf{e}_z$  and  $\mathbf{q}_z = \mathbf{e}_y$ . Physically, the quantisation axis is determined by the microwave polarisation direction with which one excites Rydberg atoms from  $|s\rangle$  to  $|p\rangle$  states, see [46].

The non-resonant vdW-Hamiltonian is set to  $\hat{H}_{\text{vdW}}(\mathbf{R}) = -1 \sum_{\alpha, \beta=1; \alpha \neq \beta}^N C_6 / (2|\mathbf{R}_{\alpha\beta}|^6)$ , assuming identical interactions for  $s$  or  $p$  states for simplicity. In reality these typically differ, which can give rise to interesting effects at shorter distances [20] that will not be relevant here.

Central to our results are the eigenstates of the electronic Hamiltonian also called Frenkel excitons [47]. We label them  $|\varphi_k(\mathbf{R})\rangle$  and the eigenenergies  $U_k(\mathbf{R})$  in  $\hat{H}_{\text{el}}(\mathbf{R})|\varphi_k(\mathbf{R})\rangle = U_k(\mathbf{R})|\varphi_k(\mathbf{R})\rangle$ . The  $U_k$  are also referred to as Born-Oppenheimer surfaces (BO surfaces).

*Initialisation:* Exactly four atoms have been Rydberg excited to the overall state  $|S\rangle = |ssss\rangle$ . We describe their random position near the laser focus positions  $\mathbf{R}_0^{(n)}$  by the initial nuclear (atomic) wave function  $\phi_{\text{nuc}}(\mathbf{R}, t=0) = (2\pi\sigma_0^2)^{-3N/4} e^{-(\mathbf{R}-\mathbf{R}_0)^2/(4\sigma_0^2)}$ , with variance  $\sigma_0 = 0.5 \mu\text{m}$ , challenging but in reach for standard techniques. After laser-excitation with a microwave linearly polarized in the  $\mathbf{q} \in \{\mathbf{e}_y, \mathbf{e}_z\}$ -direction, the Rydberg atoms are excited from the state  $|S\rangle$  to the exciton state  $|\varphi_{\text{ini}}\rangle \approx (|\pi_1, 0\rangle + |\pi_2, 0\rangle)/\sqrt{2}$ , with  $p$ -excitation localized on the horizontal Rydberg dimer and providing repulsive interactions (see also [46]). Selective excitation of this exciton is achieved by detuning the microwave frequency by the initial exciton energy  $U_{\text{ini}}(\mathbf{R}_0) \approx 22.27 \text{ MHz}$  from the  $s \rightarrow p$  transition. For  $\mathbf{q} = \mathbf{e}_y$  the state  $|\varphi_{\text{ini}}\rangle$  corresponds to the second most energetic BO surface and for  $\mathbf{q} = \mathbf{e}_z$  to the third. The mean energetic separation between these two states is only  $\Delta E = 0.57 \text{ KHz}$ , allowing a sufficiently broad microwave pulse to address both selectively with just a change of polarisation.

The full initial state of the Rydberg aggregate is then  $|\Psi_{\text{tot}}(\mathbf{R}, t=0)\rangle = \phi_{\text{nuc}}(\mathbf{R}, t=0) \otimes |\varphi_{\text{ini}}\rangle$ . The combined propagation of atomic motion and electronic excitation

dynamics with Tully's fewest switching algorithm [48–50] provides many realisations of the simulation (trajectories), each containing the time-dependent position  $\mathbf{R}(t)$  of atoms, the expansion coefficients  $c_{\alpha m}$  of the electronic state  $|\Psi(t)\rangle = \sum_{\alpha m} c_{\alpha m}(t) |\pi_{\alpha}, m\rangle$  and an index  $s(t)$  of the currently active Born-Oppenheimer surface  $U_s(\mathbf{R}(t))$  [46].

*Non-adiabatic dynamics:* Following Rydberg excitation to  $|s\rangle$  and  $|p\rangle$ , the four aggregate atoms will move essentially unperturbed through the background gas [21]. This motion takes place in three-dimensional space and is governed by anisotropic resonant dipole-dipole interactions *without any confinement*. Initially atoms 1 and 2 repel each other as sketched in FIG. 1. Eventually 2 comes closer to 3–4 setting these into motion as well, which also remains near the  $x, y$ -plane, facilitating observations. The total atomic column densities after some time of free atomic motion have an interesting multi-lobed structure, shown in FIG. 2, a central result of the present work. The essentially planar character of the motion now allows us to trace back the multiple lobes to the atomic system crossing a conical intersection (CI) [18, 25] at some slightly earlier time than shown. The crossing occurs when atoms 2–4 nearly form an equilateral triangle and results in roughly equal population on *two* of the BO surfaces of the system. Since atoms experience different forces on these surfaces, the atomic density distribution at the final time shows several clearly distinguishable peaks. Segregating trajectories according to their respective BO surface [46], the simulation allows us to unambiguously link these separate spatial features in FIG. 2 to motion on specific Born-Oppenheimer surfaces.

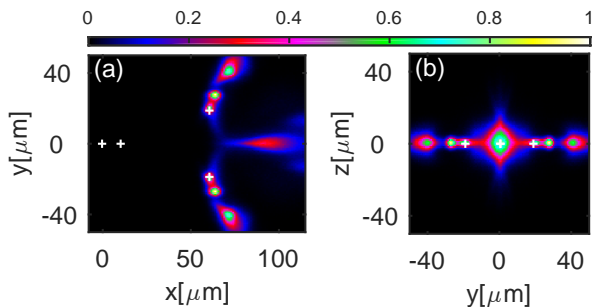


FIG. 2: (color online) Atomic density of the final state at  $t = 92.9 \mu\text{s}$ , using  $\mathbf{q} = \mathbf{e}_y$ . Shown are column densities in the  $x$ - $y$  plane (a) and  $y$ - $z$  plane (b). The white '+' mark the initial atomic positions. The maximal densities are set to 1.

Optical confinement of atoms in one-dimensional traps along with a reduction of the electronic state space assumed in our related earlier work [18, 25] constitute a significant experimental challenge. The present results show that these restrictions are not required. It is simply the symmetry of the initially prepared system which keeps the motion similarly planar and hence accessible. The successful splitting into different motional modes through

the CI is a sensitive measure for the extent to which the atomic motion remains in a plane. Our findings suggest flexible Rydberg aggregates as an experimental platform for the study of quantum chemical effects on much inflated length and time scales with presently available technologies [14, 32, 33, 51].

*Experimental signatures:* The total atom density of FIG. 2 is experimentally accessible if the focus positions  $\mathbf{R}_0^{(n)}$  are sufficiently reproducible to allow averaging over many realisations. Additionally, one requires near single atom sensitive position detection. A shot-to-shot position uncertainty  $\sigma_0$  in 3D *within* each laser focus is already taken into account in our simulation. Recent advances in position sensitive field ionisation enable  $\sim 1 \mu\text{m}$  resolution, clearly sufficient for an image such as FIG. 2. Panel (b) could alternatively also be observed by waiting for atom 3–4 to impact on a solid state detector. The

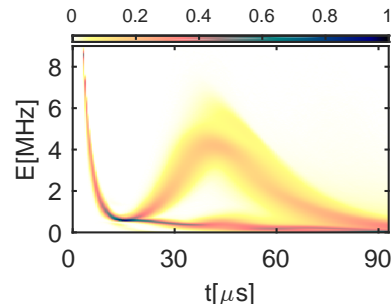


FIG. 3: (color online) Time resolved potential energy density  $u(E, t)$  (maximum set to one) as explained in the text. To emphasize low density features, we plot the square root.

background gas can also act as a probe for position and state of the embedded moving Rydberg atoms [14, 28–31], offering resolution sufficient for FIG. 2 as well.

Non-adiabatic dynamics discussed here can not only be monitored in position space, but also in the excitation spectrum of the system, similar to Ref. [32]. The observable is the time-resolved potential energy density  $u(E, t)$ , shown in FIG. 3. To obtain  $u(E, t)$  we bin the potential energy  $U_s(t)$  of the currently propagated BO-surface  $s$  into a discretized energy grid  $E$  and average over all trajectories. We see a clear splitting into several features within  $u(E, t)$  in FIG. 3. Observation of  $u(E, t)$  could proceed by monitoring the time- and frequency resolved outcome of driving the  $p \rightarrow d$  transition. Similar techniques would allow an observation of the entire exciton spectrum of the system, rather than only the currently populated state, we show averaged plots of full spectra in [46].

An alternative experiment to observe our non-adiabatic dynamics, would individually trap four atoms at positions  $\mathbf{R}_0^{(n)}$ , with trapping width  $\sigma_0$ , prior to Rydberg excitation, see e.g. [51].

*Switch Born-Oppenheimer surfaces:* The present system allows a simple handle deciding on which Born-

Oppenheimer surface the system is initialised, and consequently to what extent the subsequent evolution involves CIs and non-adiabatic effects. This handle is the linear polarisation direction of the microwave for exciton creation, which selects the exciton state that is initially excited.

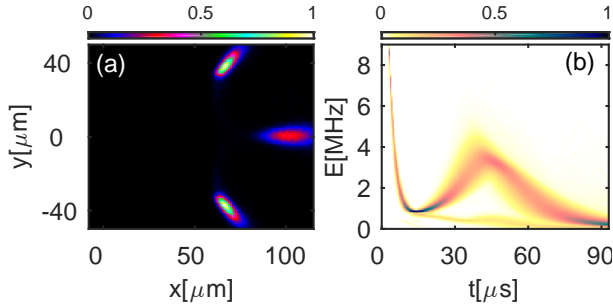


FIG. 4: (color online) Alternate dynamics for microwave polarisation direction  $\mathbf{q} \parallel \mathbf{e}_z$ . Column density in the  $x$ - $y$  plane at  $t = 92.9 \mu\text{s}$  (a), potential energy density (b).

So far we have discussed the case  $\mathbf{q} = \mathbf{e}_y$ . Choosing  $\mathbf{q} = \mathbf{e}_z$  instead allows the same  $s \rightarrow p$  excitation pulse to access a different initial BO-surface, with substantially less non-adiabaticity. This is shown in FIG. 4.

*Perturbation by ground state atoms:* We expect the dynamics of the embedded Rydberg aggregate discussed here not to be significantly perturbed by its cold gas environment. Rydberg-Rydberg interactions substantially exceed elastic Rydberg ground-state atom interactions [52, 53] for separations  $d > 200$  nm, and dipole-dipole excitation transport disregards ground state atoms [21]. Our kinetic energies of  $\mathcal{O}(10$  MHz) are still low enough to render inelastic  $\nu$  or  $l$  changing collisions very unlikely [53], leaving molecular ion- or ion pair creation as main Rydberg excitation loss channel arising from collisions with ground state atoms [53, 54]. Even including those and assuming a background gas density of  $\rho = 4 \times 10^{18} \text{ m}^{-3}$ , we can extrapolate experimental data from Rb [32] to infer a lifetime of about  $\tau = 130 \mu\text{s}$  for the embedded Rydberg aggregate here [46].

However, detrimentally large cross sections for the same processes were found in [53, 54] for much larger densities  $\rho$ . Further research on ionisation of fast Rydberg atoms within ultra cold gases is thus of interest for the present proposal.

In summary, controlled creation of a few Rydberg atoms in a cold gas of ground state atoms will allow to initiate coherent motion of the Rydberg atoms without external confinement as demonstrated here with the unconstrained motion of four Rydberg atoms, forming coupled excitonic Born-Oppenheimer surfaces. This enables non-adiabatic motional dynamics in assemblies of a few Rydberg excited atoms as an experimental platform for studies of quantum chemical processes inflated to convenient time (microseconds) and spatial (micrometers)

scales, with the perspective to shed new light on relevant processes such as ultra-fast vibrational relaxation or quantum control schemes for embedded systems. Experimental observables are atomic density distributions or exciton spectra. Different degrees of non-adiabaticity can be accessed from the same initial atomic positions through the choice of the initial exciton state.

The effects explored will be most prominent with light Alkali species, such as Li discussed here, but also the more common Rb can be used. Here a slightly smaller setup would sufficiently accelerate the motion to fit our scenario into the Rb system life-time. Rb would, however, pose a greater challenge for the theoretical modelling, making the inclusion of spin-orbit coupling necessary [41, 42].

Beyond the controlled scenario discussed here, illuminating a 3D gas entirely with a single Rydberg excitation laser, followed by microwave transitions to the  $p$  state, should also quickly result in non-adiabatic effects. They would arise through the abundant number of CIs in random 3D Rydberg assemblies [18].

We acknowledge helpful discussions with Thomas Pohl. **Supplemental material: Exciton induced directed motion of unconstrained atoms in an ultracold gas:**

*This supplemental material provides additional details regarding micro wave excitation of excitons, Tully's fewest switching algorithm, signatures of non-adiabatic effects and effects of the background gas.*

*Excitons and Born-Oppenheimer surfaces:* The eigenstates of the electronic Hamiltonian are termed Frenkel excitons [47]. We label them  $|\varphi_k(\mathbf{R})\rangle$  and the eigenenergies  $U_k(\mathbf{R})$ , thus

$$\hat{H}(\mathbf{R})|\varphi_k(\mathbf{R})\rangle = U_k(\mathbf{R})|\varphi_k(\mathbf{R})\rangle. \quad (3)$$

The  $U_k$  are also referred to as Born-Oppenheimer surfaces (BO surfaces). Since our electronic basis  $\mathcal{B}$  has  $3N$  elements for  $N$  atoms, the operator  $\hat{H}(\mathbf{R})$  is represented by a  $3N \times 3N$  matrix.

The full electronic wavefunction can be expanded in the eigenstates

$$|\psi_{\text{el}}\rangle = \sum_{k=1}^{3N} \tilde{c}_k |\varphi_k(\mathbf{R})\rangle, \quad (4)$$

where the  $\tilde{c}_n$  are called the adiabatic expansion coefficients. Since for each atomic configuration the eigenstates and the diabatic basis are linked via a unitary transformation, we are also able to expand the electronic wavefunction diabatically, i.e.

$$|\psi_{\text{el}}\rangle = \sum_{\alpha=1}^N \sum_{m=-1}^1 c_{\alpha,m} |\pi_{\alpha}, m\rangle, \quad (5)$$

with  $c_{\alpha,m}$  the diabatic coefficients.

*Microwave excitation to the initial electronic state:* With a microwave  $\mathcal{E}_0(t)$  that is linear polarized in the  $\mathbf{q}$ -direction, the aggregate can be excited from the state  $|S\rangle$  to an exciton. The Hamiltonian of the microwave-atom coupling can approximately be written as

$$\hat{H}_{\text{mw}}(t) = \mathcal{E}_0(t) \sum_{\alpha=1}^N \hat{d}_0^{(\alpha)}, \quad (6)$$

where  $\hat{d}_0^{(\alpha)}$  is the dipole operator of the  $\alpha$ th atom projected onto the polarization direction of the microwave. The relative probability to end up from state  $|S\rangle$  in a specific exciton  $|\varphi_k\rangle$  with energy  $U_k$  can be calculated via [55]

$$\mathbb{P}(|S\rangle, |\varphi_k\rangle) = \frac{|T(|S\rangle, |\varphi_k\rangle)|^2 X(U_k)}{\sum_{l=1}^{3N} |T(|S\rangle, |\varphi_l\rangle)|^2 X(U_l)}, \quad (7)$$

with  $T(|S\rangle, |\varphi\rangle) := \langle S | \hat{H}_{\text{mw}}(t) | \varphi \rangle$  the transition matrix element from  $|S\rangle \rightarrow |\varphi\rangle$  due to the microwave and  $X(E)$  the power spectral density of the microwave at energy  $E$ . Typically we can assume  $X(E)$  to be a Gaussian, centered at the microwave frequency (energy)  $\hbar\omega_{\text{mw}}$ . The transition matrix element is given by

$$T(|S\rangle, |\varphi\rangle) = \frac{\mathcal{E}_0(t)\mathfrak{d}}{\sqrt{3}} \sum_{\alpha=1}^N c_{\alpha,0}, \quad (8)$$

with  $c_{\alpha,0} = \langle \pi_{\alpha}, 0 | \varphi \rangle$  the diabatic expansion coefficients of the exciton. The initial atomic configuration is chosen, such that there are excitons localized on the horizontal Rydberg dimer which provide repulsive interactions. According to (8), the microwave can only excite to excitons with excitation oriented along the microwave polarization direction. Only for  $\mathbf{q} \in \{\mathbf{e}_y, \mathbf{e}_z\}$  there is a single repulsive exciton, localized on the horizontal Rydberg dimer, with even electronic symmetry,

$$|\varphi\rangle \approx (|\pi_1, 0\rangle + |\pi_2, 0\rangle)/\sqrt{2}. \quad (9)$$

The latter is required for the transition according to (8) to be allowed such that we can initially excite to this state,  $|\psi_{\text{el}}(t=0)\rangle = |\varphi\rangle$ , by choosing a microwave frequency of  $\omega_{\text{mw}} = 22.27$  MHz.

*Propagation:* The system is fully described with the total Hamiltonian

$$\hat{H}(\mathbf{R}) = - \sum_{n=1}^N \frac{\nabla_{\mathbf{R}_n}^2}{2M} + \hat{H}_{\text{el}}(\mathbf{R}). \quad (10)$$

For larger number of atoms, solving the time dependent Schrödinger equation following from Eq. (10) is not feasible in a reasonable time. However a quantum-classical propagation method, Tully's fewest switching algorithm [48–50], gives results in good agreement with the

full propagation of the Schrödinger equation [16, 17, 21, 25]. In Tully's fewest switching algorithm, the positions  $\mathbf{R}$  of the atoms are treated classically according to Newton's equation

$$M\ddot{\mathbf{R}} = -\nabla_{\mathbf{R}} U_s(\mathbf{R}). \quad (11)$$

Here the mechanical potential felt by the atoms corresponds to a *single* eigenenergy  $U_s$  of the electronic Hamiltonian. The index  $s$  will undergo stochastic dynamics described below, necessitating the calculation of a large number of trajectories (solutions) of (11).

Meanwhile the electronic state of the Rydberg aggregate is described quantum mechanically governing the electronic Schrödinger equation,

$$i\hbar \frac{\partial}{\partial t} |\psi_{\text{el}}(t)\rangle = \hat{H}_{\text{el}}(\mathbf{R}(t)) |\psi_{\text{el}}(t)\rangle, \quad (12)$$

where  $\mathbf{R}(t)$  enters as a parameter which by itself is the solution of (11). Specifically we solve (12) by expanding diabatically, arriving at

$$i\hbar \dot{\mathbf{c}}(t) = \mathbf{H}_{\text{el}}(\mathbf{R}(t)) \mathbf{c}(t), \quad (13)$$

with

$$\mathbf{c} = (c_{1,-1} \ c_{1,0} \ c_{1,1} \ \dots \ c_{N,-1} \ c_{N,0} \ c_{N,1})^T \quad (14)$$

and

$$\mathbf{H}_{\text{el}}(\mathbf{R}) = \begin{pmatrix} h_{1,-1;1,-1}(\mathbf{R}) & \dots & h_{1,-1;N,1}(\mathbf{R}) \\ \vdots & \dots & \vdots \\ h_{N,1;1,-1}(\mathbf{R}) & \dots & h_{N,1;N,1}(\mathbf{R}) \end{pmatrix}, \quad (15)$$

where  $h_{\alpha,m;\beta,m'}(\mathbf{R}) := \langle \pi_{\alpha}, m | \hat{H}_{\text{el}}(\mathbf{R}) | \pi_{\beta}, m' \rangle$ .

To retain further quantum properties two features are added. Firstly, the atoms are randomly placed according to the Wigner distribution of the initial nuclear wavefunction and also receive a corresponding random initial velocity. In the end of the simulation, all observables have to be averaged over the whole set of realizations. Secondly, non-adiabatic processes are added as follows: The probability for a transition from surface  $l$  to surface  $k$ , is proportional to the non-adiabatic coupling vector

$$\mathbf{d}_{kl}(\mathbf{R}) = \langle \varphi_k(\mathbf{R}) | \nabla_{\mathbf{R}} | \varphi_l(\mathbf{R}) \rangle. \quad (16)$$

Consistent with this, Tully's algorithm allows for jumps of the index  $s$ , from an energy surface  $s = l$  to an energy surface  $s = k$  during the propagation.

The sequence of propagation is as follows:

1. The initial positions of the atoms are randomly determined with the probability distribution  $|\phi_{\text{nuc}}(\mathbf{R}, t=0)|^2$ . We do the same with the velocities by using the fourier transformed probability distribution,  $\mathcal{FT}[|\phi_{\text{nuc}}(\mathbf{R}, t=0)|^2]$ .



2. The electronic Hamiltonian is diagonalized and we pick the electronic state with index  $k$  randomly according to the probability  $|\langle \varphi_{\text{ini}} | \varphi_k(\mathbf{R}_0) \rangle|^2$ , where  $|\varphi_{\text{ini}}\rangle$  is the electronic initial state defined in the main text.
3. The atomic positions are propagated one time step with (11), while states are propagated with (13).
4. We determine whether the surface index  $s$  undergoes a stochastic jump according to (16) (see [15] for the precise prescription).
5. The new positions lead to new eigenstates and -energies, thus we repeat from point 2.

*Identification of non-adiabatic effects:* To unambiguously prove that the separate density features after conical intersection crossing originate from atomic motion on separate BO surfaces, we show in FIG. 5 the same type of information, but with density data separately assembled depending on the current propagations surface  $s$  of the quantum-classical algorithm. We can clearly allocate different features to different surfaces. In addition

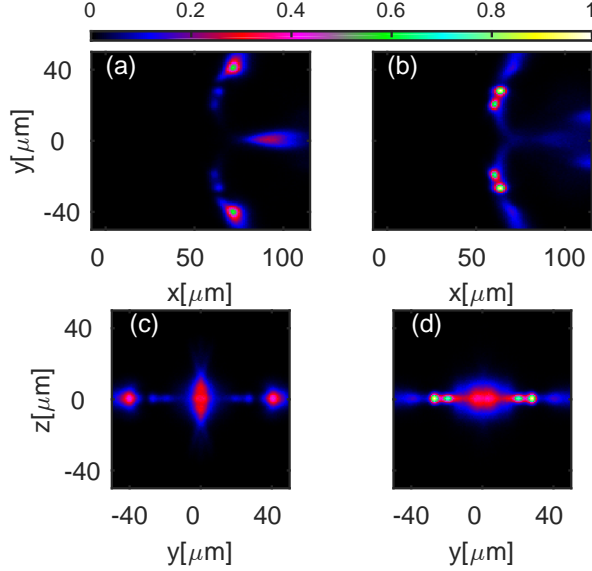


FIG. 5: (color online) The same as Fig. 2 of the main article, but with atomic density segregated by BO surfaces: (a,c) second highest BO surface, (b,d) fourth highest BO surface. (a,b) Column densities in the  $x$ - $y$  plane. (c,d) Column densities in the  $y$ - $z$  plane. We set the maximum density to one for each plot.

to spectral information about the current exciton state of the system, as discussed in the main text, also the overall exciton spectrum (with possibly unoccupied states) is experimentally accessible. We construct the corresponding exciton density of states  $g(E, t)$  analogously to  $u(E, t)$ , but now binning all eigenenergies  $U_k$  instead of only the currently propagated surface  $U_s$ .

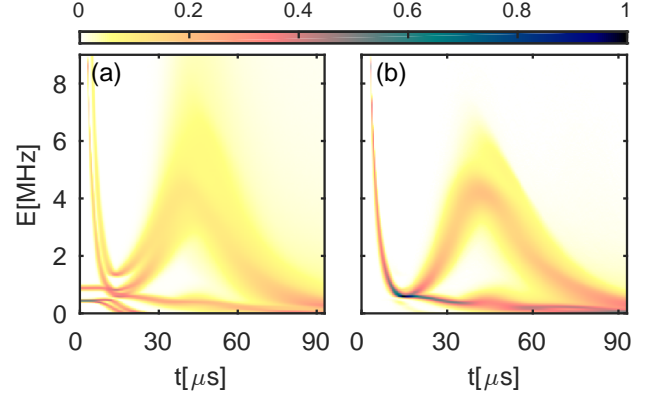


FIG. 6: (color online) (a) Time resolved exciton density of states  $g(E, t)$  and (b) potential energy density  $v(E, t)$  as in Fig. 3(z) of the main article. These spectra are also experimentally observable as in [32]. We set the maximum density to one for each plot. To emphasize low density features, we plot the square root of all quantities.

*Inelastic interactions with the background gas:* For the scenario proposed here, Rydberg excited atoms with  $\nu = 80$  in  $l = 0, 1$  states move through a background gas of ground state atoms with density  $\rho = 4 \times 10^{18} \text{ m}^{-3}$  at a maximal velocity of about  $v_{\text{ini}} \sim \sqrt{U_{\text{ini}}(R_0)}/2 \approx 0.85 \text{ m/s}$ . We can deduce a maximal cross-section for ionizing collisions between Rydberg atoms and ground state atoms of  $\sigma(\nu) = 610 \text{ nm}^2$  at  $\nu = 60$  from experiment [32]. Assuming scaling with the size of the Rydberg orbit [54], we extrapolate this value to our  $\nu = 80$ , thus  $\sigma(80) = \sigma(60)(80/60)^2 10^3 \text{ nm}^2$ .

The total decay rate of our four atom system is then  $\Gamma_{\text{tot}} = 2\Gamma_{\text{coll}} + 4\Gamma_0$ , with spontaneous decay rate  $\Gamma_0$  and collisional decay rate  $\Gamma_{\text{coll}}$  for single atoms. We have assumed that only two atoms ever move with the fastest velocity. Using  $\Gamma_{\text{coll}} = \rho v_{\text{ini}} \sigma(80)$ , we finally arrive at a total life-time  $\tau = 1/\Gamma_{\text{tot}} = 130 \mu\text{s}$  as quoted in the main text.

- 
- [1] T. F. Gallagher, *Rydberg Atoms* (Cambridge University Press, 1994).
  - [2] D. Jaksch, J. I. Cirac, P. Zoller, S. L. Rolston, R. Côté, and M. D. Lukin, Phys. Rev. Lett. **85**, 2208 (2000).
  - [3] M. D. Lukin, M. Fleischhauer, R. Côté, L. M. Duan, D. Jaksch, J. I. Cirac, and P. Zoller, Phys. Rev. Lett. **87**, 037901 (2001).
  - [4] E. Urban, T. A. Johnson, T. Henage, L. Isenhower, D. D. Yavuz, T. G. Walker, and M. Saffman, Nature Physics **5**, 110 (2009).
  - [5] A. Gaëtan, Y. Miroshnychenko, T. Wilk, A. Chotia, M. Viteau, D. Comparat, P. Pillet, A. Browaeys, and P. Grangier, Nature Physics **5**, 115 (2009).
  - [6] I. Lesanovsky and J. P. Garrahan, Phys. Rev. Lett. **111**, 215305 (2013).

- [7] R. M. W. van Bijnen and T. Pohl, Phys. Rev. Lett. **114**, 243002 (2015), URL <http://link.aps.org/doi/10.1103/PhysRevLett.114.243002>.
- [8] A. W. Glaetzle, M. Dalmonte, R. Nath, C. Gross, I. Bloch, and P. Zoller, Phys. Rev. Lett. **114**, 173002 (2015), URL <http://link.aps.org/doi/10.1103/PhysRevLett.114.173002>.
- [9] T. Wilk, A. Gaëtan, C. Evellin, J. Wolters, Y. Miroshnychenko, P. Grangier, and A. Browaeys, Phys. Rev. Lett. **104**, 010502 (2010).
- [10] M. M. Müller, M. Murphy, S. Montangero, T. Calarco, P. Grangier, and A. Browaeys, Phys. Rev. A **89**, 032334 (2014).
- [11] O. Mülken, A. Blumen, T. Amthor, C. Giese, M. Reetz-Lamour, and M. Weidemüller, Phys. Rev. Lett. **99**, 090601 (2007).
- [12] D. Barredo, H. Labuhn, S. Ravets, T. Lahaye, A. Browaeys, and C. S. Adams, Phys. Rev. Lett. **114**, 113002 (2015).
- [13] S. Bettelli, D. Maxwell, T. Fernholz, C. S. Adams, I. Lesanovsky, and C. Ates, Phys. Rev. A **88**, 043436 (2013).
- [14] G. Günter, H. Schempp, M. Robert-de-Saint-Vincent, V. Gavryusev, S. Helmrich, C. S. Hofmann, S. Whitlock, and M. Weidemüller, Science **342**, 954 (2013).
- [15] C. Ates, A. Eisfeld, and J. M. Rost, New J. Phys. **10**, 045030 (2008).
- [16] S. Wüster, C. Ates, A. Eisfeld, and J. M. Rost, Phys. Rev. Lett. **105**, 053004 (2010).
- [17] S. Möbius, S. Wüster, C. Ates, A. Eisfeld, and J. M. Rost, J. Phys. B: At. Mol. Opt. Phys. **44**, 184011 (2011).
- [18] S. Wüster, A. Eisfeld, and J. M. Rost, Phys. Rev. Lett. **106**, 153002 (2011).
- [19] S. Wüster, C. Ates, A. Eisfeld, and J. M. Rost, New J. Phys. **13**, 073044 (2011).
- [20] H. Zoubi, A. Eisfeld, and S. Wüster, Phys. Rev. A **89**, 053426 (2014).
- [21] S. Möbius, M. Genkin, S. Wüster, A. Eisfeld, and J.-M. Rost, Phys. Rev. A **88**, 012716 (2013).
- [22] S. Wüster, S. Möbius, M. Genkin, A. Eisfeld, and J.-M. Rost, Phys. Rev. A **88**, 063644 (2013).
- [23] M. Genkin, S. Wüster, S. Möbius, A. Eisfeld, and J. M. Rost, J. Phys. B: At. Mol. Opt. Phys. **47**, 095003 (2014).
- [24] S. Möbius, M. Genkin, A. Eisfeld, S. Wüster, and J. M. Rost, Phys. Rev. A **87**, 051602 (2013).
- [25] K. Leonhardt, S. Wüster, and J. M. Rost, Phys. Rev. Lett. **113**, 223001 (2014).
- [26] W. Domcke, D. R. Yarkony, and H. Köppel, *Conical Intersections* (World Scientific, 2004).
- [27] A. J. White, U. Peskin, and M. Galperin, Phys. Rev. B **88**, 205424 (2013), URL <http://link.aps.org/doi/10.1103/PhysRevB.88.205424>.
- [28] B. Olmos, W. Li, S. Hofferberth, and I. Lesanovsky, Phys. Rev. A **84**, 041607(R) (2011).
- [29] G. Günter, M. R. de Saint-Vincent, H. Schempp, C. S. Hofmann, S. Whitlock, and M. Weidemüller, Phys. Rev. Lett. **108**, 013002 (2012).
- [30] D. W. Schönleber, A. Eisfeld, M. Genkin, S. Whitlock, and S. Wüster, Phys. Rev. Lett. **114**, 123005 (2015).
- [31] H. Schempp, G. Günter, S. Wüster, M. Weidemüller, and S. Whitlock, Phys. Rev. Lett. **115**, 093002 (2015).
- [32] R. C. Teixeira, C. Hermann-Avigliano, T. L. Nguyen, T. Cantat-Moltrecht, J. M. Raimond, S. Haroche, S. Gleyzes, and M. Brune, Phys. Rev. Lett. **115**, 013001 (2015).
- [33] N. Thaicharoen, A. Schwarzkopf, and G. Raithel (2015), arXiv:1506.02705.
- [34] A. Fioretti, D. Comparat, C. Drag, T. F. Gallagher, and P. Pillet, Phys. Rev. Lett. **82**, 1839 (1999), URL <http://link.aps.org/doi/10.1103/PhysRevLett.82.1839>.
- [35] W. Li, P. J. Tanner, and T. F. Gallagher, Phys. Rev. Lett. **94**, 173001 (2005), URL <http://link.aps.org/doi/10.1103/PhysRevLett.94.173001>.
- [36] M. Mudrich, N. Zahzam, T. Vogt, D. Comparat, and P. Pillet, Phys. Rev. Lett. **95**, 233002 (2005), URL <http://link.aps.org/doi/10.1103/PhysRevLett.95.233002>.
- [37] L. G. Marcassa, A. L. de Oliveira, M. Weidemüller, and V. S. Bagnato, Phys. Rev. A **71**, 054701 (2005), URL <http://link.aps.org/doi/10.1103/PhysRevA.71.054701>.
- [38] V. A. Nascimento, M. Reetz-Lamour, L. L. Caliri, A. L. de Oliveira, and L. G. Marcassa, Phys. Rev. A **73**, 034703 (2006), URL <http://link.aps.org/doi/10.1103/PhysRevA.73.034703>.
- [39] T. Amthor, M. Reetz-Lamour, S. Westermann, J. Denskat, and M. Weidemüller, Phys. Rev. Lett. **98**, 023004 (2007), URL <http://link.aps.org/doi/10.1103/PhysRevLett.98.023004>.
- [40] T. Amthor, M. Reetz-Lamour, C. Giese, and M. Weidemüller, Phys. Rev. A **76**, 054702 (2007), URL <http://link.aps.org/doi/10.1103/PhysRevA.76.054702>.
- [41] H. Park, P. J. Tanner, B. J. Claessens, E. S. Shuman, and T. F. Gallagher, Phys. Rev. A **84**, 022704 (2011).
- [42] H. Park, E. S. Shuman, and T. F. Gallagher, Phys. Rev. A **84**, 052708 (2011).
- [43] P. Goy, J. Liang, M. Gross, and S. Haroche, Phys. Rev. A **34**, 2889 (1986).
- [44] K. Leonhardt, S. Wüster, and J. M. Rost (2015), physics.atom-ph/1511.06629.
- [45] F. Robicheaux, J. V. Hernandez, T. Topcu, and L. D. Noordam, Phys. Rev. A **70**, 042703 (2004).
- [46] See Supplemental Material at [URL will be inserted by publisher] for more technical details.
- [47] J. Frenkel, Phys. Rev. **37**, 17 (1931).
- [48] J. C. Tully and R. K. Preston, J. Chem. Phys. **55**, 562 (1971).
- [49] S. Hammes-Schiffer and J. C. Tully, J. Chem. Phys. **101**, 4657 (1994).
- [50] M. Barbatti, Wiley Interdisciplinary Reviews-Computational Molecular Science **1**, 620 (2011).
- [51] F. Nogrette, H. Labuhn, S. Ravets, D. Barredo, L. Béguin, A. Vernier, T. Lahaye, and A. Browaeys, Phys. Rev. X **4**, 021034 (2014).
- [52] C. H. Greene, A. S. Dickinson, and H. R. Sadeghpour, Phys. Rev. Lett. **85**, 2458 (2000).
- [53] J. B. Balewski, A. T. Krupp, A. Gaj, D. Peter, H. P. Büchler, R. Löw, S. Hofferberth, and T. Pfau, Nature **502**, 664 (2013).
- [54] T. Niederprüm, O. Thomas, T. Manthey, T. M. Weber, and H. Ott, Phys. Rev. Lett. **115**, 013003 (2015).
- [55] We use  $U_k \ll \hbar\omega_{mw}$ .